oceans

MDPI

Article

Spring Phytoplankton Bloom Phenology in the Bering Sea and Surrounding Waters Based on MODIS Data

Kirill Kivva [1,*], Aleksandra Malysheva [1,2] and Aleksandra Sumkina [1]

[1] Russian Federal Research Institute of Fisheries and Oceanography, Moscow 105187, Russia; malysheva@vniro.ru (A.M.); sumkina@vniro.ru (A.S.)
[2] Department of Oceanology, Faculty of Geography, Lomonosov Moscow State University, Moscow 119991, Russia
* Correspondence: kivva@vniro.ru

Abstract

The Bering Sea and its surrounding waters are commercially and ecologically important ecosystems. Knowledge of phytoplankton phenology is crucial for understanding ecosystem dynamics. However, estimates of phenological parameters of spring phytoplankton bloom are sparse for this region. We used the Moderate Resolution Imaging Spectroradiometer (MODIS) daily data from 2003–2024 to assess the climatology of phenological parameters. A combination of data regriding, spatial interpolation, and temporal smoothing was applied. Three methods of spatial interpolation for missing data acquisition are compared: iterative first-order neighbor, inverse distance weighted interpolation, and data interpolating empirical orthogonal functions (DINEOF). We suggest that the first outcompetes the other two methods when compared to initial data. Date of the bloom initiation, bloom peak, chlorophyll-a maximum, and duration of the bloom before its peak are evaluated. The spatial distribution of mentioned phenological parameters is presented and discussed. We show that bloom starts early in Bristol Bay, in the narrow band along the eastern shelf, along the Kamchatka Peninsula, and south of the Aleutians and Alaska Peninsula. In the deep Bering Sea, bloom starts surprisingly later considering the latitude of the region. The main reason for this may be the wind mixing during the spring. The first phase of the bloom is generally longer in the deep southern areas (up to 60 days) and shorter in the northern shelf areas (less than 2 weeks in some cases).

Keywords: Bering Sea; spring phytoplankton bloom; phenology; bloom initiation; bloom duration; climatology; spatial distribution; spatial interpolation; MODIS; DINEOF

Check for updates

Academic Editor: Santiago Hernández-León

Received: 14 October 2025
Revised: 18 January 2026
Accepted: 3 February 2026
Published: 26 February 2026

Copyright: © 2026 by the authors. Licensee MDPI, Basel, Switzerland. This article is an open access article distributed under the terms and conditions of the Creative Commons Attribution (CC BY) license.

1. Introduction

1.1. Importance of Phytoplankton Bloom

Spring phytoplankton bloom (SPB) contributes more than 50% of the total annual new primary production in many Arctic and Subarctic marine ecosystems [1–3]. The organic matter formed during the spring bloom feeds all heterotrophic organisms in the ecosystem, including commercially important fishes and invertebrates [4]. In temperate and polar regions, the bloom conditions, including its phenological characteristics, may influence the share of the organic matter transported to the bottom, a primary driver of pelagic–benthic coupling [4,5]. The timing of the bloom itself may influence the survival of fish, including commercial species, at early life stages [6–8]. Therefore, information on the bloom initiation and termination timing, its physical conditions, and its biological consequences is essential

for understanding inter-annual ecosystem changes, as well as for comprehensive fisheries management. Such information may also be important for tasks related to carbon fluxes assessment at the sea–atmosphere interface [9].

Given the importance of such data, numerous research efforts have already addressed questions related to SPB timing variability and its factors in the World Ocean or specific ocean regions, e.g., ref. [10–12]. Most of the recent research on this topic relies on remotely sensed data on chlorophyll-a concentration (Chl-a), as satellites provide regular and long-term measurements for wide areas of the ocean.

1.2. The Region of Interest

The Bering Sea is one of the largest marginal seas [13] located in the subpolar geographic zone (Figure 1). Approximately half of the sea area is a shelf, which is wide in the eastern part of the sea (500–800 km) and narrow along the western coast (30–120 km). The deep-water region, the so-called 'oceanic domain' of the sea, is connected through deep straits with the Pacific Ocean. The orographic diversity of the seabed, together with spatial scales and transitional Arctic–temperate location, results in substantial seascape diversity and considerable multi-year variability of physical factors within the sea [14]. Some sea regions are among the most productive marine ecosystems [15–18]. On the other hand, the 'oceanic domain' is generally a more oligotrophic region [19].

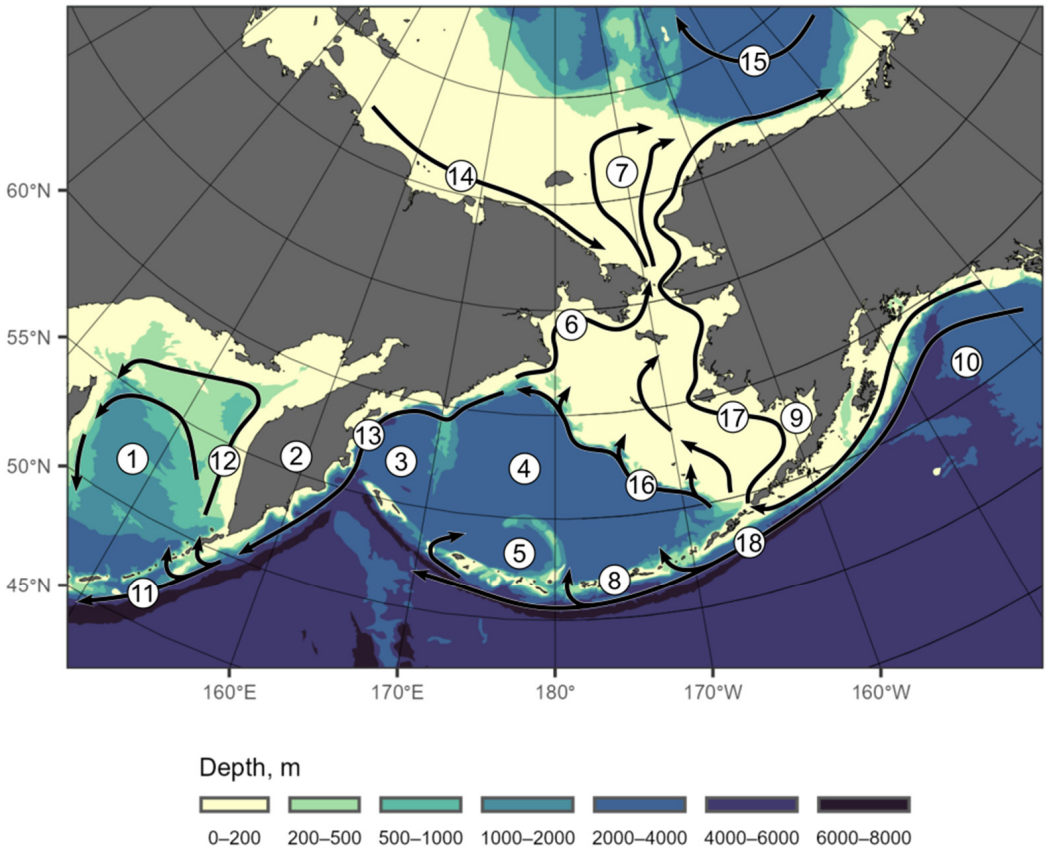


Figure 1. Bathymetry (shading) and main surface currents (arrows) of the Bering Sea and surrounding waters. Numbers indicate main geographical objects and currents: (1) Sea of Okhotsk, (2) Kamchatka Peninsula, (3) Komandorski (Commander) Basin, (4) Aleutian Basin, (5) Bowers Basin, (6) Gulf of Anadyr and Anadyr Current, (7) Chukchi Sea, (8) Aleutian Islands, (9) Bristol Bay, (10) Gulf of Alaska, (11) North Kuril Current, (12) West Kamchatka Current, (13) East Kamchatka Current, (14) Siberian Coastal Current, (15) Beaufort Gyre, (16) Bering Slope Current, (17) Alaskan Coastal Current, (18) Alaskan Stream. Currents are based on generalization of [14,33]. Bathymetry is generalized based on GEBCO_2023.

The Bering Sea supports a substantial commercial fishery that contributes about 40% of the US catches and about 10–15% of Russian catches by volume [20,21]. The most important commercial fish species of the Bering Sea include walleye pollock, Pacific cod, Pacific herring, and Pacific salmon such as pink salmon and sockeye salmon, all of which depend on zooplankton as prey and may be potentially influenced by phytoplankton bloom conditions at their early life stages [6,22–25].

Although this study is focused mostly on the Bering Sea, it is important to look at the broader region in order to put our findings into wider context. Therefore, here we analyze data from 50–70° N, 150° E–150° W. This region covers part of the Arctic Ocean including the Chukchi Sea, which is similar to the northern Bering Sea in terms of drastic climate change and sufficient spatial and temporal shifts in ecosystem components from plankton through higher trophic levels [26–30]. The study area also embraces the eastern Sea of Okhotsk, another highly important fishery region (e.g., ref. [31]). The southern edge of the region of interest spans part of the North Pacific Ocean, which is also important for commercial fish migration (e.g., ref. [32]). An additional reason for including part of the North Pacific in the analysis is the possibility to compare our data with multiple previous research efforts (see Section 1.3 and 4.1).

1.3. Status of Knowledge

The data on SPB phenology in the region of interest, particularly in the Bering Sea, are still sparse. Several previous research efforts focused on the Bering Sea only briefly touched the timing of Chl-a maximum based on monthly data [34,35] or reported the date of maximum primary production based on remote sensing data [19]. Several studies looked at the connection between sea ice and SPB timing, but they covered only parts of our region of interest [36,37]. A recent study illustrated the timing of the Chl-a maximum in more detail, but at a lower resolution and only for the Bering Sea shelf area east of 180° E [11]. Another recent paper investigated the climatology of SPB phenology for the North Pacific, excluding the marginal seas and areas along the Aleutians [38]. Chl-a dynamics in the Sea of Okhotsk, including phenological parameters, received substantially less attention compared to the Bering Sea or Pacific Arctic. Only a general description of seasonal Chl-a dynamics and SPB phenology is available to date [39–41]. Existing pan-Arctic research focused on phytoplankton bloom presented a climatology of SPB peak timing in the area north of 50° N [42], but their results were obtained after Chl-a data approximation using the Gaussian model; thus, they are largely smoothed. Research projects focused on the phytoplankton bloom phenology in the entire World Ocean usually exclude the Bering Sea area due to lack of data [10,12]. Moreover, they usually have coarse spatial resolution.

This brief analysis allows us to conclude that information on SPB phenology in the region of interest is fragmentary and mostly based on data of low spatial or temporal resolution. Sufficient information on SPB timing in the western Bering Sea is still absent. This paper particularly aims to fill these knowledge gaps.

1.4. Objective and Scope

This research is a part of a broader project focused on SPB timing variability and physical factors. The main objective of this particular work is to develop a framework for SPB phenology research in the Bering Sea based on satellite data. We also present here the first assessment of SPB phenological parameters' spatial variability in the entire sea and surrounding regions. The tasks of the work include the search for the most suitable combination of spatial data binning and interpolation as well as temporal data smoothing.

2. Materials and Methods

2.1. Chl-a Data

This research employs the Moderate Resolution Imaging Spectroradiometer (MODIS) data on Chl-a from the Aqua satellite available from the NASA Ocean Biology Distributed Active Archive Center (http://oceancolor.gsfc.nasa.gov/, accessed on 16 December 2025). We used the standard Chl-a data product based on the OC3M algorithm. It has been noted previously that the OC3M algorithm is sufficiently good for most of our areas of interest, at least for phytoplankton phenology assessment [34]. Only very coastal regions close to the river mouths may have high concentrations of chromophoric (colored) dissolved organic matter, which may influence Chl-a estimates based on remotely sensed data [43,44]. The nominal spatial resolution of the data product is 4 km, and the temporal resolution is 1 day. All available full years of data were used (2003–2024). As winter data are virtually absent for the area of interest, only data between 31st of January and 26th of November were considered for each year. The data was downloaded in NetCDF format.

2.2. Spatial Data Binning

Remotely sensed Chl-a data, which are based on measurements in visible wavelength bands, are subject to gaps depending on cloud and sea ice conditions, as well as the sun angle. The Bering Sea and surrounding areas almost entirely lie within the 'blind spot' for visible imagery satellite instruments during the winter months, and sea ice and clouds substantially limit data availability during the rest of the year. Spatial data binning (regriding) is one of the most common techniques used for acquisition of Chl-a datasets with fewer gaps. However, the balance between bin size and the characteristic spatial scales of the region under study should be carefully considered, as larger bins allow one to obtain a data array with fewer or even no gaps, although smaller bins are desirable in terms of spatial variability analysis and visualization [45].

For instance, spatial latitudinal-longitudinal bins of $0.5^\circ \times 1.0^\circ$ were used in recent research focused on the eastern Bering Sea [11]. The disadvantage of using latitudinal-longitudinal bins is their area dependence on latitude, which is especially substantial in high-latitude regions such as the Bering Sea. As a result, spatial bins in the northern and southern parts of the area may have different initial data loads, which can potentially influence the results, as southern bins can incorporate more data compared to the northern bins. Moreover, the $0.5^\circ \times 1.0^\circ$ spatial resolution leads to relatively coarse results (e.g., see Figure 3 in [11]). One possible solution is to use equal-area grid cells.

As SPB timing is shown to be related to the sea ice conditions [8,19,46,47], it is further necessary to determine a convenient method of combined analysis of Chl-a data and sea-ice data. One of the most consistent data products on sea-ice concentration with the longest time-series is the NOAA/NSIDC Climate Data Record of Passive Microwave Sea Ice Concentration (NOAA/NSIDC CDR) [48]. This product employs an equal-area spatial grid with cells of 25×25 km. This spatial resolution is higher than that used by [11] (approximately 50×50 km), so if used for Chl-a, it will allow for more detailed results on the Bering Sea SPB timing. At the same time, it is substantially lower than the initial resolution of the MODIS Chl-a data, which suggests a sufficient increase in the share of filled grid cells after regriding. A similar spatial resolution was employed by several recent studies in the field of phytoplankton phenology [45,49], which supports the validity of such an approach. Therefore, the NOAA/NSIDC CDR grid was used in this study for spatial data binning and subsequent spatial interpolation as it has equal area cells, sufficiently high resolution, and allows for analysis of ice influence on Chl-a in further research.

The resulting value for each grid cell was calculated as the median of all data entries for three days (date and two neighboring days) from a particular cell. Note that the stars

R package treats each initial data point as a polygon (rectangular in latitude-longitude coordinate system and quadrangle after applying the equal-area coordinate reference system). This means that, in the case that a particular initial data pixel covers the grid cell vertex or cell side, this initial data unit may contribute to up to four grid cells. Considering the initial data is pixels, this approach is more organic compared to the method of treating initial MODIS data as spatial points.

2.3. Missing Value Acquisition with Spatial Interpolation

Spatial interpolation was used for missing values acquisition after the initial data were log-transformed. Three spatial interpolation methods were used and compared. One of them is the custom iterative first-order neighbor (IFON) averaging method. At each iteration of the algorithm, the grid cells with missing data but with at least two neighboring and opposite to each other cells with data were found. Such cells with missing data were filled with the mean of values from all (not necessarily only two) first-order neighboring cells. The algorithm was repeated until fewer than 1000 grid cells were filled in a certain year during the iteration (note that this value is arbitrary). Six or seven iterations were run for each particular year. Counting all dates of a particular year, the total number of filled cells in each year was between 120,107 and 146,813. The use of this method ensures that gap filling is strictly based on nearby cells' data and wide areas of missing values are not completely filled. This allows one to increase the reliability of gap filling.

The second method used for missing values acquisition is inverse distance weighted (IDW) interpolation. This method uses data weighting based on spatial distance; the closer the data point, the higher weight it has [50,51]. IDW is one of the most common interpolation techniques, and it was previously used for applications related to missing Chl-a values acquisition [52].

IDW was carried out with the function idw from the R package gstat. In order to prevent complete filling of wide areas of missing values, the radius of the data search for interpolation was set to 50 km. The data values were weighted to the square of the distance.

The third method used for filling the missing data is data interpolating empirical orthogonal functions (DINEOF), one of the most common modern techniques for spatial data interpolation [53–56]. This method is based on identification of dominant patterns in a given multidimensional dataset. We apply the function dineof from the R package sinkr [57]. DINEOF fills all data gaps, including winter values from northern regions covered with ice, and those values are often obviously overestimated (e.g., 10–15 mg/m^3 in the Arctic in winter). Therefore, we exclude all the values before the beginning of the MODIS time-series and after the end of the time-series for a particular grid cell in particular year. This allowed us to avoid unreasonable data extrapolation.

The number of filled data gaps was calculated for each day and visualized for each year, separately for each of the three interpolation methods.

In order to assess the quality of missing data acquisition, 30% of values, or about 3300 randomly chosen grid cells, were artificially removed from spatially binned data sets and were filled (if possible) using the three methods. The resulting filled values were compared to the initial values using visual analysis, as well as metrics, including root-mean square error (RMSE) and coefficient of variation (R^2). Visual comparison of the spatial interpolation methods was additionally carried out for the number of random dates.

2.4. Temporal Smoothing

Many missing values were still present in most grid cells each year even after spatial interpolation. The cells with less than 50 data values in a particular year were excluded from further analysis. Relatively high-frequency and large-amplitude variability is a well-

known characteristic of Chl-a data, particularly for the Bering Sea [34]. This is a cause of substantial difficulties when estimating the phenological parameters. In order to overcome this limitation and to additionally fill data gaps, temporal smoothing with interpolation was carried out using locally estimated scatterplot smoothing (LOESS, function loess from the R package stats). Several values of the parameter span (α), which controls the smoothing degree, were tested manually on multiple randomly chosen grid cells and years. This parameter was set to 0.2 based on expert analysis. This means that 20% of the entire time-series was used for the calculation of fit value at each point. This function implies tricubic weighting for each data entry, meaning the closest data points have higher weight.

Note that we are not aware of any implementation of LOESS smoothing in previous similar research (see Section 4.4 for discussion). The use of LOESS is preferable in the case of the Bering Sea region due to the presence of substantial data gaps and high Chl-a variability.

2.5. Phenological Parameters Assessment

The most common phenological parameters recently used to describe SPB in marine environments include the date of SPB start or initiation (date of bloom initiation, DBI); the date of Chl-a maximum, also called bloom peak timing (date of chlorophyll-a maximum, DCM); and the date of SPB termination (date of bloom termination, DBT) [10,12]. An additional parameter is the duration of the bloom (BD), which is commonly assessed as the difference between DBT and DBI. We assessed all of these parameters except for DBT, as it is difficult to evaluate in the case of the Bering Sea where SPB may be followed by several immediate summer Chl-a splashes and the subsequent fall bloom, which are often impossible to precisely identify (see Section 4.4 for more details). Therefore, in this study, we evaluated the duration of the bloom through the duration of its first phase between the initiation and timing of the maximum concentration, i.e., BD = DCM − DBI. We additionally estimated the Chl-a maximum value (CM).

In order to estimate phenological parameters, the following procedure was carried out for each particular cell for each year. In cases where the first data point was after 19th of July (a relatively frequent situation for the ice-covered northern regions), CM and DCM were calculated using full time-series. In the opposite case, only data from before 1st of August were used for the calculation of CM and DCM to focus specifically on the SPB, but not on possible autumn bloom, which is known to start in September–October in our area of interest [8,18]. This limitation is particularly important for the deep regions of the Bering Sea, where autumn bloom may be even more pronounced compared to the spring bloom in some years [58]. In cases where the DCM was less than 10 days from the beginning of the time-series, the other phenological parameters were not calculated. This may be the case when Chl-a data was absent during the early phase of bloom due to sea ice or clouds and thus considering such situations may result in erroneous values of DBI. If the time interval between the start of the time-series and DCM was at least 10 days, the DBI was estimated using the median threshold method. The median was calculated based only on the data before DCM. Note that in most previous research, the median was calculated using data for the entire year or even entire multi-year time-series, and a value of the median times 1.1 or similar was used as a threshold [12,59–62]. In the case of the Bering Sea, the inter-annual variability of Chl-a in a particular grid cell may be quite high depending on the geographical location. This is why different years should be treated separately. Moreover, high values of Chl-a may be observed throughout summer, and autumn phytoplankton bloom may occur in September–November. Therefore, using full-year data for calculation of the SPB threshold in many regions of the Bering Sea is irrational.

2.6. Software Used for the Analysis

All data manipulations were carried out using R version 4.4.1 [63] with the packages stars (reading and processing of NetCDF files) [64], dplyr (pipelines and general data operations) [65,66], lubridate (operations with dates) [67], sf (spatial data operations) [68], and gstat (spatial interpolation) [69]. Data were transformed into North Pole Lambert equal-area projection for the Bering Sea (EPSG:3571). All figures were prepared in R with the package ggplot2 [70]. All maps in this article are created using EPSG:3571.

3. Results

3.1. Description of Binning and Interpolation Results

The area of the Bering Sea and surrounding waters is often covered by clouds, regardless of the season, and partially covered by sea ice (note that the most northern regions are often covered by ice year-round). That is why remote-sensing Chl-a data are often unavailable for large portions of the region under study.

When considering regrided data, the highest share of dates with data (about 60%) is general characteristic of the waters east of the Kamchatka Peninsula and south of the Alaska Peninsula (Figure 2a). In most parts of the Bering Sea, the initial share of dates with data is about 40–50%, and Chl-a data is available for only 10–20% of dates in the northern part of the study region.

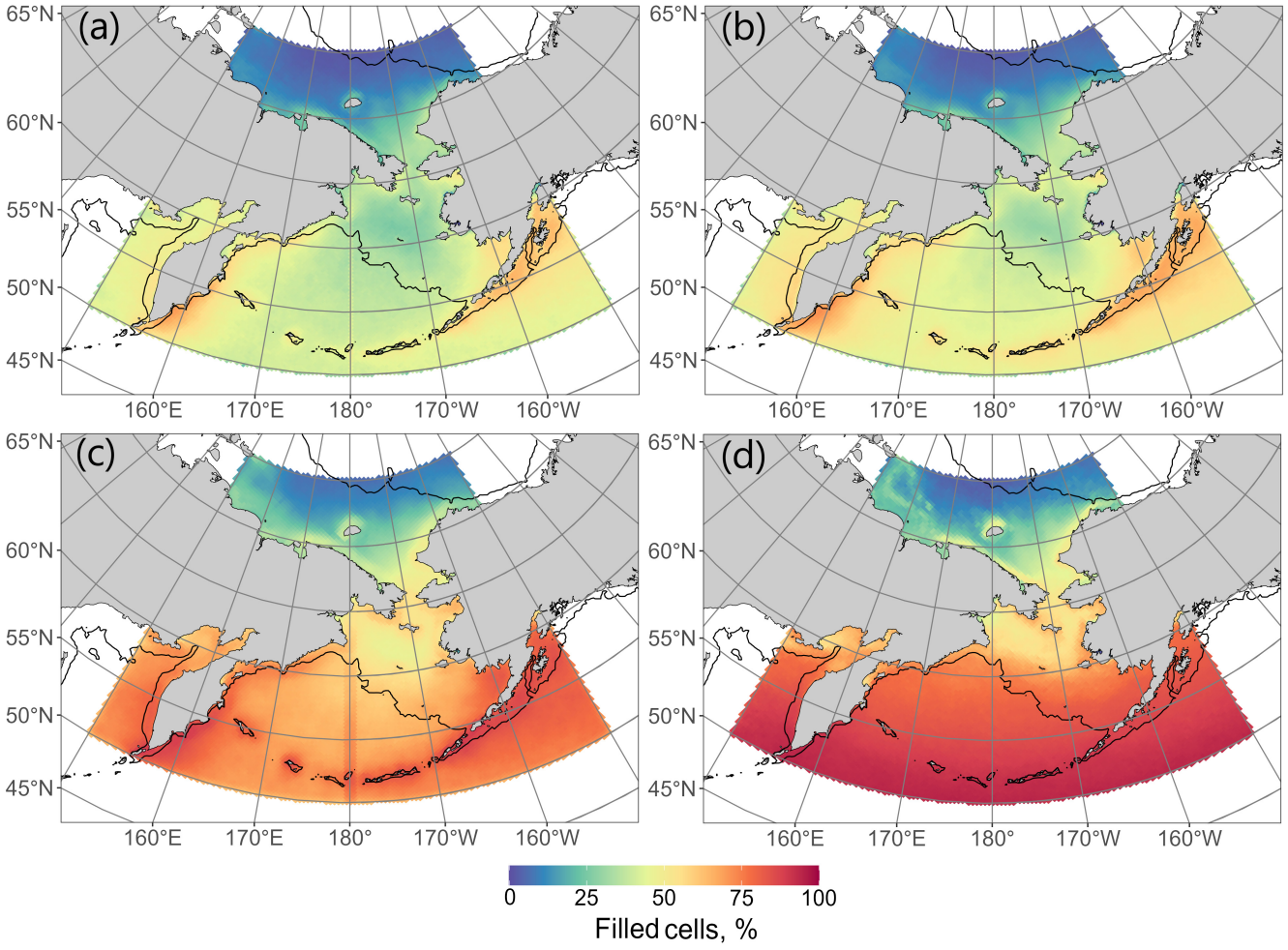


Figure 2. Proportion of dates with data for 2003–2024, percent of 6622 days (22 years of 301 days): (**a**) initial dataset, (**b**) after iterative first-order neighbor (IFON) interpolation, (**c**) after inverse distance weighted (IDW) interpolation, and (**d**) after DINEOF interpolation. Black lines indicate 200 m isobath.

The region-wide multi-year (2003–2024) mean annual variability of the share of data-filled cells demonstrates two periods of annual increase (Figure 3). In December and January, the share of cells with data is close to zero not only due to clouds and sea ice, but also due to a low sun angle in most parts of the study area. This share increases to 30–45% by the end of March and fluctuates in approximately this range until August, with slightly lower values in June–July. The time period between the end of August and the beginning of November usually has the highest number of grid cells with data (up to 65%). There is an obvious high variability in the share of cells with data throughout the year depending, most likely, on atmospheric synoptic processes, which largely control the cloudiness.

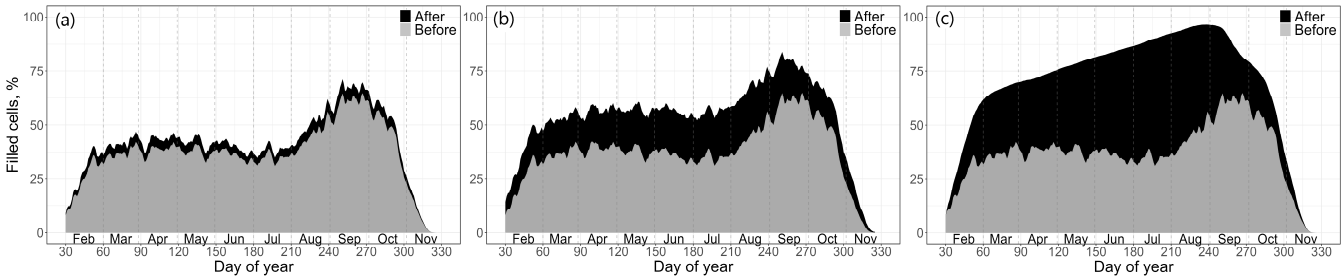


Figure 3. Multi-year mean annual variability of the share of data-filled cells before and after spatial data interpolation, based on all data from 2003–2024, percent of 11,048 cells. Grey fill shows initial share of data-filled cells before interpolation. Black fill shows share of data-filled cells after (**a**) iterative first-order neighbor (IFON) interpolation and (**b**) inverse distance weighted (IDW) interpolation, and (**c**) after DINEOF interpolation.

Interpolation allowed us to fill the missing data at least partly. IFON interpolation resulted in an increase in the share of data-filled cells by only 3–7% depending on the particular date (Figures 2b and 3a). This method leaves large lacunas unfilled by data. On the other hand, IDW interpolation allows us to fill additional 5–25% of cells with data (Figures 2c and 3b). Note that the increase in the share of data-filled cells after interpolation will be higher in the case of relaxation of limitations on the spatial range of the IDW. Applying DINEOF resulted in a substantial increase of data-filled cells (25–40%) (Figures 2d and 3c).

The spatial scale of lacunas in the data is often comparable to the entire region area (Figure 4, top row). Particular examples show a modest but reasonable amount of missing values filled by IFON (second row in Figure 4). On the other hand, IDW and DINEOF resulted in relatively high Chl-a values (1–5 mg/m^3) in areas where the initial data were absent and background Chl-a could be low (two bottom rows in Figure 4). Some particular examples presented in the figure include regions in the southern Bering Sea and along the Kamchatka Peninsula in May 2019, across the southeastern Bering Sea inner shelf and coastal southwestern Chukchi Sea in August 2024, as well as an area in the Aleutian Basin (e.g., noticeable spot of Chl-a values more than 10 mg/m^3 in IDW results) and in Karaginsky Gulf (DINEOF results) in October 2023 (see Figure S1 in Supplementary Material).

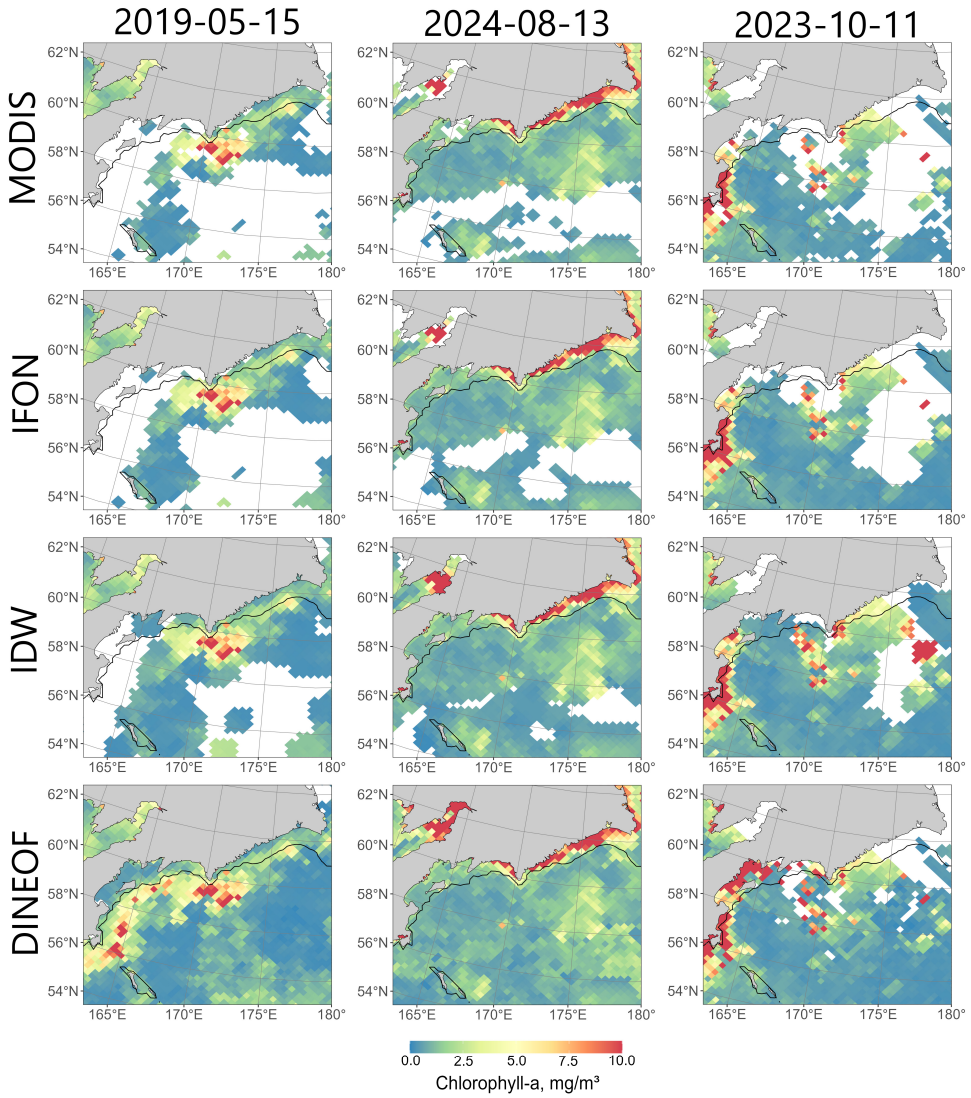


Figure 4. Examples of chlorophyll-a data interpolation for 15 May 2019 (**left column**), 11 October 2023 (**middle column**), and 13 August 2024 (**right column**). Regrided initial data (**top row**), results of iterative first-order neighbor (IFON) interpolation (**second row**), results of inverse distance weighted (IDW) interpolation (**third row**), and results of DINEOF (**bottom row**). Black lines indicate isobath 200 m.

3.2. Quality of Missing Data Acquisition

The quality of missing data acquisition was assessed both statistically and visually. All variants of test-interpolated data had a relatively wide range of deviation from the initial values (see example in Figure 5). When considering only values below 3 mg/m^3 (approximate 90th percentile of the initial data), most of the interpolated values correspond reasonably well to the initial data. However, the higher values are often underestimated by all interpolation methods under consideration. This is evident from the position of the linear regression line, which falls below the 1:1 ratio line starting approximately from 1 mg/m^3 (Figure 5). Therefore, the results should be interpreted with caution, especially in areas where spring–summer Chl-a values are anticipated to be above 1 mg/m^3. This may particularly affect our estimates of the Chl-a maximum value during the bloom, but it should not significantly affect other phenological parameters.

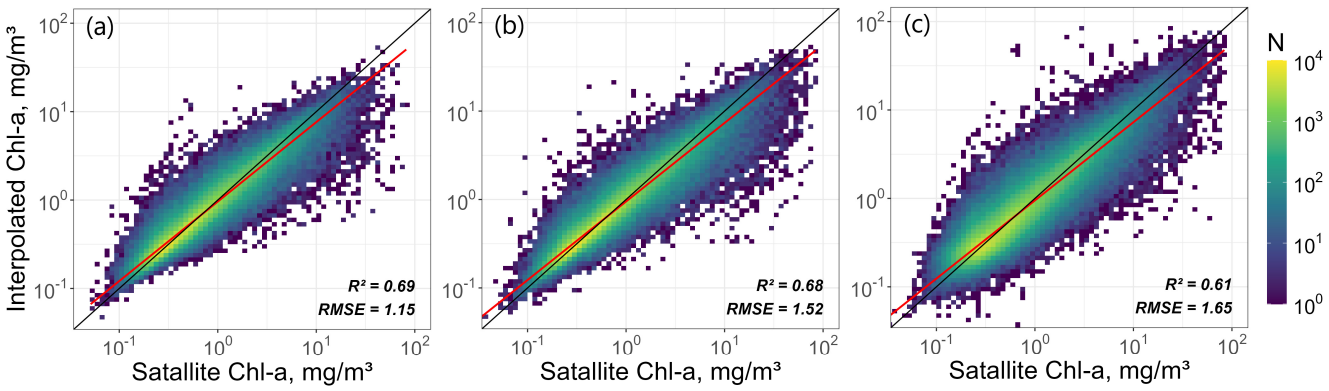


Figure 5. Examples of Chl-a data interpolation quality assessment for 2015. Comparison of initial satellite values (abscissa, mg/m^3) and interpolated values (ordinate, mg/m^3) for (**a**) iterative first-order neighbor interpolation (IFON), (**b**) inverse distance weighted interpolation (IDW), and (**c**) for DINEOF interpolation. Black line is 1:1 ratio. Red line is linear regression. Filling denotes number of data points per regular bins. Note log-scale of all axes.

When compared to the initial data, the results of the IFON interpolation showed almost the same R^2 values as the IDW interpolation (about 0.7). At the same time, the RMSE of the latter method was considerably higher (about 1.1 mg/m^3 for IFON and about 1.5 mg/m^3 for IDW). The DINEOF interpolation resulted in the lowest R^2 values (about 0.6) and highest RMSE (usually above 1.6 mg/m^3) compared to the other two methods. This result may be due to the high initial share of missed data values. DINEOF, as a data-driven method, depends strongly on input values, and therefore may return erroneous results in cases when information for dominated pattern calculation is insufficient (see Section 4.3 for discussion). Considering this, we exclude results of this particular DINEOF realization from further investigation and focus on the results of IFON and IDW only.

3.3. Date of Bloom Initiation

As our time-series are relatively short (i.e., 22 years) and phenological parameters considered may have substantial interannual variability with potential outliers, we use medians to describe climatology instead of using mean values. The distribution of phenological parameters estimated after two different interpolation methods is generally similar; therefore, only the results of IFON interpolation are shown in the pictures.

The median of DBI shows the earliest start of the bloom in Bristol Bay and the surrounding portion of the south-western Bering Sea shelf (beginning of April) (Figure 6a). Similar DBI values are characteristic of waters south of the Aleutian Islands, as well as west and east of the Kamchatka Peninsula and in the Bowers Basin. In the 'oceanic domain' of the Bering Sea, e.g., in the offshore portions of the Aleutian Basin and Komandorski Basin, the climatological value of DBI is about the middle of May. The latest median values of DBI (end of June to middle of July) were observed in the inner part of the Gulf of Anadyr and of Norton Sound (north-eastern-most gulf of the Bering Sea), western and northern periphery of the Chukchi Sea, and coastal part of the East Siberian Sea. Note that the data from the offshore portion of the East Siberian Sea are absent.

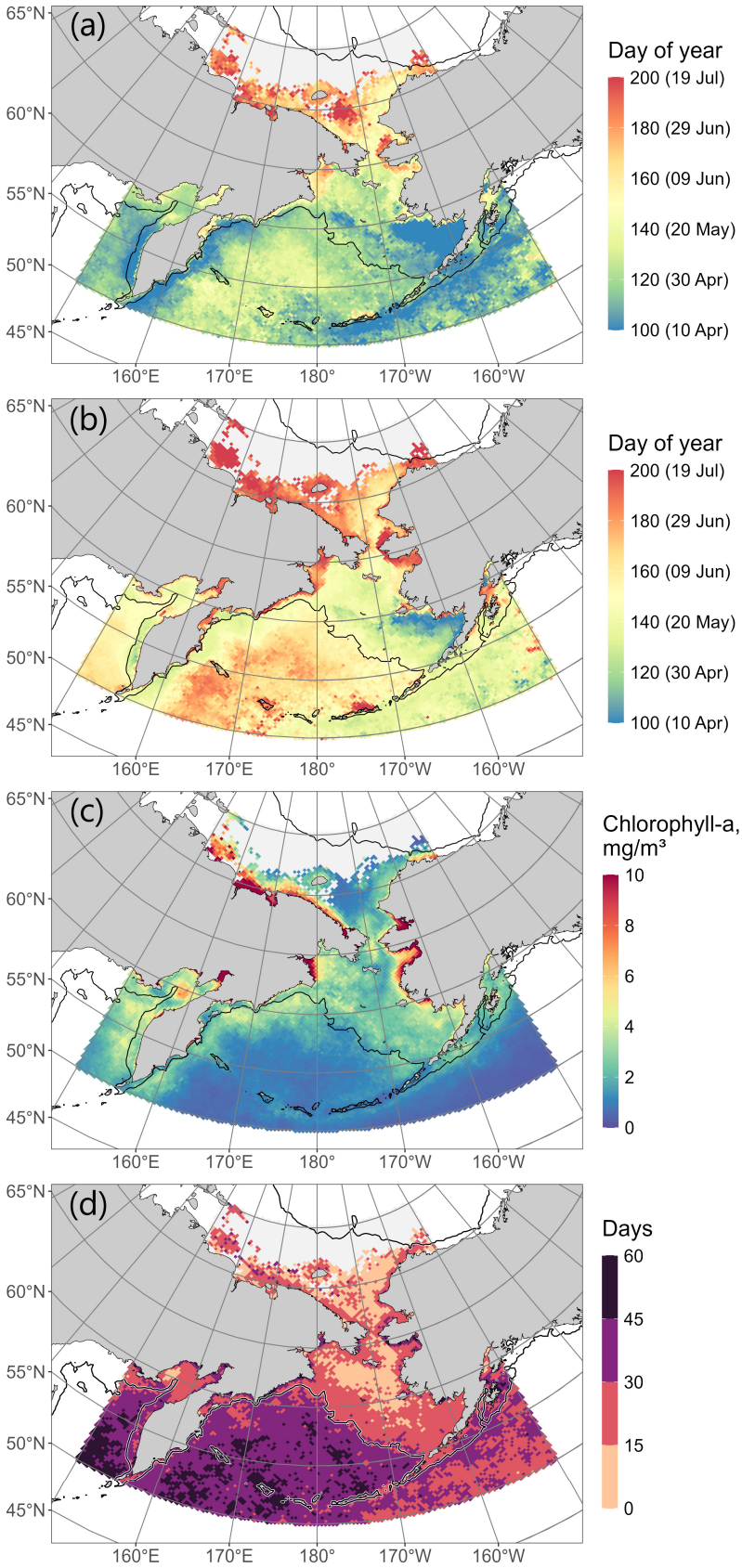


Figure 6. Climatology of phenological parameters of spring phytoplankton bloom based on results of iterative first-order neighbor interpolation (IFON). Date of spring bloom initiation (DBI) (**a**); date of maximum chlorophyll-a concentration (DCM) (**b**); chlorophyll-a maximum concentration (CM), mg/m^3 (**c**); bloom duration (BD), days (**d**). Light-gray shading indicates absence of data. Black line shows isobath 200 m.

3.4. Date of Bloom Peak Timing

In general, the distribution of the multi-year median date of Chl-a maximum is similar to the distribution of the median date of bloom initiation. However, in contrast to the DBI distribution, the map of DCM climatology demonstrates the earliest dates of Chl-a maximum (beginning of April) in Bristol Bay, with substantially later dates (early-to-mid May) along the Kamchatka Peninsula, the Aleutians, and the Alaska Peninsula (Figure 6b). Similar to the multi-year median DBI spatial pattern, the latest median DCM values (second half of July) were observed in the inner part of the Gulf of Anadyr, Norton Sound, periphery of the Chukchi Sea, and East Siberian Sea. Similar late median DCM values were also observed in the Pyasina Bay (north-eastern Sea of Okhotsk) and in the narrow coastal band along eastern Kamchatka, including the Karaginsky Gulf and the coast between Cape Olyutorsky and Cape Navarin (western Bering Sea).

3.5. Maximum Chl-a Concentration

The characteristic (multi-year median) maximum concentration of chlorophyll-a (CM) during the spring phytoplankton bloom is (not surprisingly) higher along the continental shelf and slope in the Bering Sea (more than 1.5 mg/m^3) compared to deep ocean areas (in many cases less than 1 mg/m^3) (Figure 6c). This was anticipated, as the so-called 'green belt' along the continental slope and outer shelf of the Bering Sea has consistently higher Chl-a concentrations compared to the deep regions and inner shelf [34,71]. Nevertheless, the highest values (more than 10 mg/m^3) are observed in the embayments close to the river mouth areas, e.g., Pyasina Bay, western Gulf of Anadyr, Norton Sound, and Kotzebue Sound (south-eastern Chukchi Sea), as well as along coast of the East Siberian Sea. Note, however, that those values may be overestimated due to the potential high concentration of chromophoric (colored) dissolved organic matter (see Section 2.1).

3.6. Duration of the Bloom

The median duration of the first phase of the spring phytoplankton bloom is short in the northern regions (generally less than 30 days north of 60° N) and long (more than 45 days) in the southern oceanic waters (Figure 6d). The shortest blooms (less than 15 days between initiation and the timing of Chl-a maximum) are usually observed in the northern Bering Sea and Chukchi Sea. Another characteristic feature of the BD field is the almost precise overlap of the continental shelf and the area with BD values less than 30 days.

3.7. Comparison of SPB Parameters Climatology Based on IFON and IDW Interpolation

The multi-year median dates of bloom initiation, dates of Chl-a maximum, and bloom duration assessed after IFON interpolation were generally in good agreement with the values after IDW interpolation. Medians of all these parameters differed between two methods by less than 15 days in most grid cells (see Supplementary Material for details, Figure S2).

The median Chl-a maximum values were often lower after IDW interpolation than after IFON interpolation (Figure S2c); for instance, the first and third quartiles of the difference were 0.05 and 0.38 mg/m^3, meaning more than two-thirds of the grid cells had lower maximum Chl-a after IDW than after IFON.

3.8. Dispersion of SPB Parameters

Considering the relatively short sample length in each grid cell (22 years of annual values), possible violation of normality, and presence of outliers, we use 10–90 percentile ranges in order to assess dispersion.

The 10–90 percentile ranges of dates of bloom initiation, dates of Chl-a maximum, and bloom duration assessed after IFON interpolation were highest along the southern edge

of the study area as well as in the 'oceanic' domain of the Bering Sea and along the coast (Figure S3). The characteristic values are about 80–120 days for dates of bloom initiation and Chl-a maximum, and about 45–60 days for bloom duration. This result illustrates substantial inter-annual variability of the SPB timing in the 'oceanic' part of the area of interest. That is, in some regions of the study, SPB initiation varies by 2–3 months depending on the year. The same metric of these parameters was lowest along the eastern shelf of the Bering Sea, in the Shelikhov Gulf (northeastern Sea of Okhotsk), and along the Arctic seas. The characteristic values there were in the range of 20–40 days for dates of bloom initiation and Chl-a maximum, and about 15–20 days for bloom duration (Figure S3).

The 10–90 percentile range of the Chl-a maximum value exhibits different spatial distribution. The lowest dispersion (less than 2 mg/m^3) is characteristic of the deep 'oceanic' regions, and higher dispersion is observed along the western continental slope, the outer and northern Bering Sea shelf, along the Siberian coast, in the Norton Sound, and in the Kotzebue Sound (Figure S3d).

4. Discussion

4.1. General Agreement with Previously Published Data

This research is the first attempt to illustrate the multi-year climatological pattern of the timing of the spring phytoplankton bloom initiation, as well as the maximum Chl-a values and duration of the spring phytoplankton bloom for the entire Bering Sea and surrounding waters. As was mentioned in Section 1.3, previous studies focused on the SPB phenology in the region are fragmentary and sparse. Nevertheless, previously published data allow to compare our results at least partly.

Despite the results of [12] having considerably lower resolution (5° × 8°), our data roughly agree with them in terms of the timing of bloom initiation and the timing of the bloom peak (their Figure 1) in the southern part of our study region. Similar results on the start date of the bloom are presented in [10] (their Figure 2). Our results also agree well with the data of [11] regarding the timing of the Chl-a maximum within the eastern shelf of the Bering Sea (their Figure 3). Our results on the climatological date of Chl-a maximum generally agree with the map of the month of maximum Chl-a by [35], but note that they used data only from 1998–2002 and were not focused on phenological parameters directly. Similarly, our climatological date of Chl-a maximum qualitatively agrees with the date of maximum net primary production estimated based on Sea-Viewing Wide Field-of-View Sensor (SeaWiFS) data [19]. However, the results of Brown et al. (2011) [19] suggest a substantially earlier bloom peak (end of May–beginning of June) in the deep part of the sea. This difference may be due to their time-series length (1998–2007) and the methodology of primary production estimation. Our results on DBI and CM agree well with the 'start of the first bloom' and 'Chl-a maximum value during the main bloom' of [38] (their Figure 4a,h). As mentioned above, our results support the idea of a bloom wave diverging from the band of the earliest bloom to the areas north-east and south of this band [34].

4.2. Main Patterns of Phytoplankton Bloom Phenology in the Bering Sea

Spring phytoplankton bloom in the temperate and high latitudes is known to depend on physical conditions such as light availability in the upper mixed layer and the vertical extension of the mixed layer. These parameters are influenced by the sun angle, cloudiness, and sea ice conditions, which often severely limit light penetration into the sea, as well as convective or wind mixing [6,72–76]. Therefore, it is intuitive to anticipate latitudinal distribution of the spring phytoplankton bloom phenological parameters similar to the distribution of the mentioned physical factors. However, the spatial distribution of bloom initiation and peak timing climatology revealed in this study show substantial deviation

from the latitudinal zonality. There is a band of earliest bloom stretching from eastern Kamchatka along the western continental slope and inner eastern shelf toward Bristol Bay. Both southward and northward of this area, bloom starts later. This pattern was previously described using monthly data and compared to the wave slowly propagating southward and northward [34]. The apparent reason for such strong sectoral zonality, which completely masks anticipated latitudinal zonality, is the nature of the deep 'oceanic' part of the Bering Sea. It is relatively widely accepted that this region is a high-nutrient low-chlorophyll regime controlled by labile iron availability [58,77,78]. It is similar in this regard to the Pacific Subpolar Gyre region located to the south of the Bering Sea [77,79,80]. The 'oceanic' region differs from the Bering Sea shelf and inshore areas in terms of phytoplankton composition [58]. A recent study reported a relatively subtle role of diatoms in the oceanic part of our area of interest, up to 45% in the area of the Alaskan Stream and only about 20–30% in the rest of the area [81]. At the same time, the diatom contribution to the phytoplankton community in the northern Bering and Chukchi Sea in summer may be up to 60–80% [82]. Despite these obvious dissimilarities, the exact reason for the phenological deviations between the inshore and offshore Bering Sea is still unclear. Wind mixing in late spring and early summer may be the key controlling factor [34].

Unlike the other phenological parameters considered, there is a generally geographically zonal behavior of the spring phytoplankton bloom duration. The overall pattern is that BD is decreasing northward (latitudinal zonality) and shoreward (sectoral zonality); a similar combination of latitudinal zonality and morphologically driven sectoral zonality is well known for the terrestrial landscapes [83]. The shorter bloom in northern regions means smaller proportion of energy available for the pelagic part of the ecosystem compared to the deep 'oceanic' domain of the Bering Sea and surrounding Pacific Ocean [5]. Previous studies suggest that quickly developing phytoplankton biomass largely sinks to the bottom and serves as a food source for benthos [5,19,84]. In other words, shorter blooms are more favorable for the benthic part of the ecosystem compared to the longer blooms, which are consumed by zooplankton in the pelagic layers.

4.3. Questions of Data Interpolation Quality

In this study, the iterative first-order neighbor (IFON) interpolation, inverse distance weighted (IDW), and DINEOF interpolation methods are compared with respect to the acquisition of Chl-a missing values and phenological parameters based on augmented Chl-a data. IFON is a modification of the usual nearest neighbor interpolation with additional conditions, i.e., only data from very bordering cells are considered and at least two geographically opposite cells with data should be present. The method is repeated several times, which allows one to fill more data gaps. In this study, the IDW is used with a restriction on the data search radius (50 km). Both methods resulted in similar R^2. RMSE was sufficiently higher for IDW (about 1.5 mg/m^3) compared to IFON (about 1.1 mg/m^3). At the same time, IDW allowed us to fill wider data gaps and worked comparatively faster. However, even with spatial restriction used, IDW fills relatively wide areas of missing data with interpolated values based solely on nearby and often sparse data. Even if one cell with data is present within a wide area of no-data, the employed version of IDW will produce the same values in multiple surrounding cells. Therefore, there is a general concern about precarious missing data acquisition using IDW interpolation.

DINEOF was also applied for data interpolation but showed a sufficiently lower ability in data acquisition compared with IFON and IDW. This is perhaps due to the large number of missing values. In the employed version of DINEOF, the dominating patterns of time-series were evaluated across the entire study area. Considering the diverse nature of the geographic domain of the study in terms of Chl-a dynamics, it is not surprising

that simple DINEOF implementation often resulted in erroneous values of Chl-a. Spatial restriction of data input for DINEOF, similar to what was done for IDW in this study, may potentially solve this issue. The development of DINEOF implementation with spatial restriction on input data may be considered in future research.

In order to collect more arguments in favor of one or another of the interpolation methods used in this study, we additionally compare the results of phenological parameters climatology estimation by means of relative difference, i.e., the absolute difference between methods divided by the estimation based on one of them. As far as the results of IFON are less different from the initial Chl-a values when compared to IDW, we use estimates based on IFON as the reference for the relative difference. The larger the relative difference, the larger is the deviation associated with the method under comparison (IDW in our case).

The relative differences in the climatological date of bloom initiation and the date of Chl-a maximum are between −0.05 and 0.05 (i.e., less than 5% difference) in most grid cells (68 and 83% of cases, respectively). The 90% CI of relative difference of DBI was in the range [−0.12, 0.06], and the 90% CI for DBM relative difference was even smaller. However, note that the characteristic values of these parameters range from 100 to 180 for the bloom start and from 130 to 200 for the date of maximum concentration. This means that the absolute difference in, say, 10 days, which may be a sufficient time in terms of ecosystem functioning, will result in a modest relative difference.

The 90% CI of the relative difference of BD evaluations was in the range [−0.26, 0.4] (Figure 7a). This means that in many cases the difference between the two methods may be more than 30%. More precisely, more than 20% of the grid cells showed a change in BD of more than ±20% when assessed by IFON compared to when assessed by IDW. This is the brightest illustration of the potential difference between interpolation methods in terms of phenological parameters assessed after spatial interpolation. Note that the difference in bloom duration of 20–30% may potentially indicate a significant difference in primary production and its fate [5,19,84]. Therefore, it is of high importance to have a correct estimation of bloom duration in order to better understand the ecosystem dynamics in the region of interest.

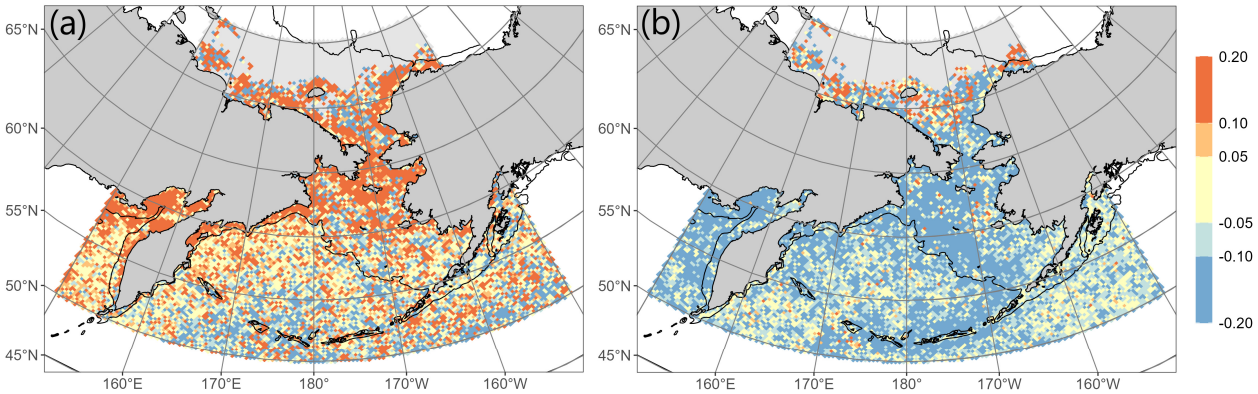


Figure 7. Relative difference of the duration of bloom first phase (**a**) and Chl-a maximum (**b**); calculated as difference between multi-year median values based on two interpolation methods (IFON result minus IDW result) divided by results based on IFON interpolation, unitless.

The 90% CI of the relative difference between the climatology of Chl-a maximum values estimated by the two interpolation methods was in the range [−0.3, 0.08], indicating a modest overall difference between the two methods (Figure 7b). However, few regions had high absolute relative differences. For instance, the climatology of the Chl-a maximum was 20% or more higher when assessed after IDW compared to values after IFON interpolation in many grid cells of the eastern Okhotsk Sea, along the shelf of the Bering Sea, and

in waters around the Aleutians. The opposite was observed in the coastal areas of the Arctic seas.

Therefore, the results of the relative difference of phenological parameters illustrate the necessity of careful choice of interpolation approach in order to better estimate the real values of phenological parameters. Considering the lower RMSE values of Chl-a compared to the initial data, we suggest that IFON interpolation outcompetes IDW in our case. Thus, we conclude that phenological parameters based on results after IFON interpolation are more realistic in our case.

In this research, three data interpolation methods are employed and evaluated, including a custom version of first-order neighbor IFON, IDW with spatial restriction on input data, and basic DINEOF. The first two of these are quite intuitive as they involve only data from the nearest neighbor cells and relatively simple operations. Similar approaches have been used in several studies, e.g., refs. [49,50,85]. However, they rely heavily on the surrounding values and are not able to capture any non-linearities. DINEOF has been previously shown to work well in many other regions [55,56,86], but we show here that simple implementation of this method for the Bering Sea area is irrational. Other potentially powerful methods for Chl-a missing data acquisition include Kriging and machine learning methods, particularly those based on neural networks [55,87–90]. The ability of these methods in capturing Chl-a variability in the Bering Sea may be tested in the future research.

4.4. Approach to Definition of the Phenological Parameters

Unlike in many recent studies aimed at phenological parameter estimation in marine environments, we used daily Chl-a data instead of using 8-day composites, e.g., refs. [10,12,85,87]. This gives an advantage of better resolved bloom timing but also amplifies the challenge of missing data acquisition. This problem is solved by spatial data interpolation and consequential temporal data smoothing and interpolation with LOESS. Spatial data interpolation is widely used in research based on satellite Chl-a, e.g., refs. [12,85,88,91,92]. Temporal data smoothing is also commonly used in such studies in the form of statistical modeling or running mean, e.g., refs. [12,49]. Despite LOESS being used previously for Chl-a data smoothing [93], we are not aware of any research that uses LOESS for Chl-a data temporal interpolation and smoothing in phenological studies. Nevertheless, we may conclude this combination of methods allowed us to obtain physically consistent results.

We used an equal-area spatial grid with cells of 25 km $\times$ 25 km. This is a relatively uncommon solution with regard to marine phenological studies both in terms of spatial resolution and shape of the grid. Note, however, that this resolution was used recently by [45]. Multiple recent research efforts have employed satellite data in their original resolution without any spatial data aggregation, e.g., refs. [61,84,87,94–96]. In such studies, the data availability problem is partly solved by using temporal composites or reduction of dimensionality by calculation of multi-year climatology of Chl-a seasonal variability. Another frequently used approach is spatial data binning using relatively large latitudinal-longitudinal bins, e.g., refs. [10,11,97]. We showed that the combination of data binning into the middle-resolution grid and consequent data interpolation allows for consistent result even when the initial data are temporarily sparse.

There are multiple different ways of determining the marine phytoplankton bloom phenological parameters. Most of the recent phenological studies use the threshold method for ascertainment of the timing of bloom initiation and termination, e.g., refs. [12,59,62,85]. Multi-year or full-year Chl-a median multiplied by a number between 1.05 and 1.15 is used as a threshold most frequently. Such an approach is not the best for the Bering Sea

and surrounding waters due to at least two circumstances. First, the Bering Sea is quite heterogeneous in terms of environment and, therefore, of Chl-a seasonal evolution. At least two distinct regimes are constantly present in this area: a high-nutrient low-chlorophyll regime and a shelf high-productivity regime. The transition zone between them is highly variable both in space and time. This means that the same place may be influenced by any of those regimes depending on the circulation pattern of a particular year or other factors, which is especially important for the deep regions close to the continental slope. This dictates the necessity of using an individual threshold in every grid cell every year. The second peculiarity of the region under consideration in regard to Chl-a seasonal dynamics is high Chl-a values after the spring bloom during summer and autumn, e.g., refs. [34,58]. Note that the winter values are often missing. The use of full-year time-series in the calculation of the threshold value in such a case will result in a higher threshold value and later estimated bloom initiation. Therefore, we applied a local median as a threshold based on data between the time-series beginning and the time of maximum spring–summer Chl-a concentration. Although not present in previous research, this approach allowed the estimation of the timing of bloom initiation.

A high level and significant temporal variability of the Chl-a concentration in summer in the Bering Sea additionally limits the calculation of the spring bloom termination timing. It is often difficult to determine the end of a spring bloom as it may be directly followed by or even merged with the summer chlorophyll splashes or autumn bloom. The only possible way to overcome this limitation is the use of a combination of several well-tuned and probably spatially variable conditions on temporal Chl-a dynamics. This issue should be addressed in further studies.

5. Conclusions

We present the first area-wide estimates of the climatology of basic phenological parameters for the entire Bering Sea and surrounding waters. Our results are based on 22 years of MODIS remote-sensed Chl-a data of daily temporal resolution. As the initial data have substantial gaps, we use a combination of spatial data binning into equal-area grid cells (25 km × 25 km), spatial data interpolation, and temporal data smoothing with simultaneous interpolation. A similar combination was previously used in Chl-a phenological research of the Southern Ocean [49], as well as of entire World Ocean [45].

We compare three spatial interpolation methods. First, the iterative first-order neighbor (IFON) interpolation, which considers only very bordering grid cells when at least two opposite cells with data are present. The method is repeated until a small number of data gaps are filled in a particular year (we use an arbitrary value of 1000 data cells). The method allowed the filling of 3–7% of grid cells with data. Second, we apply inverse distance weighted (IDW) interpolation with restriction on the radius of data search (50 km). This method allowed more gaps in the data to be filled (in most cases, more than 20% of initial grid cells). Third, DINEOF interpolation, which resulted in an increase of data-filled cells by 25–40%. We assess the quality of interpolation using test runs where 30% of grid cells are randomly chosen and the existing initial Chl-a values are compared to the interpolated values. Results show similar R^2 values of about 0.7, but lower RMSE values after IFON interpolation (about 1.1 mg/m^3) compared to the IDW interpolation (about 1.5 mg/m^3). DINEOF results had the lowest R^2 values and highest RMSE, perhaps because of too many data gaps. Therefore, we excluded DINEOF results from analysis and used IFON as the basic method for phenology calculation. We also compare the results of IFON to those of IDW.

We assessed the spring bloom start (initiation) and peak dates, as well as the Chl-a maximum value and bloom duration, a time interval between the start and peak. As was

reported in previous studies [8,11,19], the earliest bloom initiation and peak is achieved in April in the Bristol Bay. The bloom starts similarly early along the east and west coasts of the Kamchatka Peninsula, in the narrow band along the middle eastern shelf of the Bering Sea, and in the band south of Aleutians. In the deep 'oceanic' domain and in most parts of the Bering Sea shelf, the bloom starts in May. In the most northern parts of the Bering Sea, the bloom starts in June. In the Chukchi and East Siberian Seas, this happens in late June or July. The bloom duration follows zonal law. The first phase of the bloom is generally longer in the southern deep regions and shorter in the shelf northern areas. The maximum values of Chl-a are generally higher along the 'green belt' of the Bering Sea and in the shelf areas compared to the deep regions, which is consistent with previous reports [34,71].

We additionally conclude that the Chl-a interpolation method should be selected with caution as it may substantially influence the results. For instance, the duration of the bloom deviated by 20% or more in 20% of the grid cells when assessed after IDW interpolation compared to IFON interpolation. Such a difference may be significant for ecosystem research.

Finally, we suggest testing Kriging and machine learning as additional methods of Chl-a data interpolation and missing data acquisition. The next steps should also include a search for physical mechanisms responsible for the bloom initiation in the Bering Sea and surrounding waters. The exact mechanisms of the spring bloom are particularly unclear for the 'oceanic domain' of the Bering Sea, where the bloom start is surprisingly late considering its latitude. Further directions of Chl-a phenological studies in the Bering Sea may also include an updated method for spring bloom termination date estimation and research on autumn bloom phenology.

Supplementary Materials: The following supporting information can be downloaded at: https://www.mdpi.com/article/10.3390/oceans7020021/s1, Figure S1: Examples of chlorophyll-a data interpolation for 15 May 2019 (left column), 11 October 2023 (middle column) and 13 August 2024 (right column). Regrided initial data (top row), results of iterative first order neighbor (IFON) interpolation (second row), results of Inverse Distance Weighted (IDW) interpolation (third row), and results of DINEOF (bottom row). Black lines indicate isobath 200 m.; Figure S2: Difference of multi-year median values of spring phytoplankton bloom phenological parameters between IFON and IDW methods (IFON minus IDW). Difference of date of spring bloom initiation (DBI) (a), days; date of maximum chlorophyll-a concentration (DCM) (b), days; chlorophyll-a maximum concentration (CM) (c), mg/m3; bloom duration (BD) (d), days. Light-gray shading indicates absence of data. Black lines indicate isobath 200 m.; Figure S3: 10–90 percentile range of four spring phytoplankton bloom phenological parameters based on results of iterative first order neighbor interpolation (IFON) from 2003–2024. Date of spring bloom initiation (DBI) (a); date of maximum chlorophyll-a concentration (DCM) (b); bloom duration (BD), days (c); chlorophyll-a maximum concentration (CM), mg/m3 (d). Light-gray shading indicates absence of data. Black line shows isobath 200 m.

Author Contributions: Conceptualization, K.K.; methodology, K.K. and A.M.; software, K.K. and A.M.; validation, K.K. and A.M.; formal analysis, K.K.; investigation, K.K.; resources, K.K.; data curation, A.M. and A.S.; writing—original draft preparation, K.K.; writing—review and editing, A.M. and A.S.; visualization, K.K. and A.M.; supervision, K.K. All authors have read and agreed to the published version of the manuscript.

Funding: This research was funded by Russian Science Foundation, project № 25-27-00385.

Data Availability Statement: MODIS data on Chl-a is available through http://oceancolor.gsfc.nasa.gov/ (accessed on 16 December 2025). Resulted data on phenological parameters are available upon request from A.M. and K.K.

Conflicts of Interest: The authors declare no conflicts of interest.

Abbreviations

The following abbreviations are used in this manuscript:

SPB	Spring phytoplankton bloom
Chl-a	Chlorophyll-a concentration
MODIS	Moderate Resolution Imaging Spectroradiometer
IFON	Iterative first-order neighbor averaging method
IDW	Inverse distance weighted method
RMSE	Root-mean square error
LOESS	Locally estimated scatterplot smoothing
DBI	Date of bloom initiation
DCM	Date of chlorophyll-a maximum
DBT	Date of bloom termination
BD	Duration of the bloom
CM	Chlorophyll-a maximum value

References

1. Leu, E.; Mundy, C.; Assmy, P.; Campbell, K.; Gabrielsen, T.; Gosselin, M.; Juul-Pedersen, T.; Gradinger, R. Arctic Spring Awakening—Steering Principles behind the Phenology of Vernal Ice Algae Blooms. *Prog. Oceanogr.* **2015**, *139*, 151–170. [CrossRef]
2. Nielsen, J.M.; Pelland, N.A.; Bell, S.W.; Lomas, M.W.; Eisner, L.B.; Stabeno, P.; Harpold, C.; Stalin, S.; Mordy, C.W. Seasonal Dynamics of Primary Production in the Southeastern Bering Sea Assessed Using Continuous Temporal and Vertical Dissolved Oxygen and Chlorophyll-a Measurements. *J. Geophys. Res. Ocean.* **2023**, *128*, e2022JC019076. [CrossRef]
3. Wassmann, P.; Reigstad, M.; Haug, T.; Rudels, B.; Carroll, M.L.; Hop, H.; Gabrielsen, G.W.; Falk-Petersen, S.; Denisenko, S.G.; Arashkevich, E.; et al. Food Webs and Carbon Flux in the Barents Sea. *Prog. Oceanogr.* **2006**, *71*, 232–287. [CrossRef]
4. Mueter, F.; Iken, K.; Cooper, L.; Grebmeier, J.; Kuletz, K.; Hopcroft, R.; Danielson, S.; Collins, E.; Cushing, D. Changes in Diversity and Species Composition Across Multiple Assemblages in the Eastern Chukchi Sea During Two Contrasting Years Are Consistent with Borealization. *Oceanography* **2021**, *34*, 38–51. [CrossRef]
5. Grebmeier, J.M. Shifting Patterns of Life in the Pacific Arctic and Sub-Arctic Seas. *Annu. Rev. Mar. Sci.* **2012**, *4*, 63–78. [CrossRef] [PubMed]
6. Hunt, G.L., Jr.; Coyle, K.O.; Eisner, L.B.; Farley, E.V.; Heintz, R.A.; Mueter, F.; Napp, J.M.; Overland, J.E.; Ressler, P.H.; Salo, S.; et al. Climate Impacts on Eastern Bering Sea Foodwebs: A Synthesis of New Data and an Assessment of the Oscillating Control Hypothesis. *ICES J. Mar. Sci.* **2011**, *68*, 1230–1243. [CrossRef]
7. Platt, T.; Fuentes-Yaco, C.; Frank, K.T. Spring Algal Bloom and Larval Fish Survival. *Nature* **2003**, *423*, 398–399. [CrossRef]
8. Sigler, M.F.; Stabeno, P.J.; Eisner, L.B.; Napp, J.M.; Mueter, F.J. Spring and Fall Phytoplankton Blooms in a Productive Subarctic Ecosystem, the Eastern Bering Sea, during 1995–2011. *Deep Sea Res. Part II Top. Stud. Oceanogr.* **2014**, *109*, 71–83. [CrossRef]
9. Behrenfeld, M.J.; Boss, E.S. Resurrecting the Ecological Underpinnings of Ocean Plankton Blooms. *Annu. Rev. Mar. Sci.* **2014**, *6*, 167–194. [CrossRef]
10. Friedland, K.D.; Mouw, C.B.; Asch, R.G.; Ferreira, A.S.A.; Henson, S.; Hyde, K.J.W.; Morse, R.E.; Thomas, A.C.; Brady, D.C. Phenology and Time Series Trends of the Dominant Seasonal Phytoplankton Bloom across Global Scales. *Glob. Ecol. Biogeogr.* **2018**, *27*, 551–569. [CrossRef]
11. Nielsen, J.M.; Sigler, M.F.; Eisner, L.B.; Watson, J.T.; Rogers, L.A.; Bell, S.W.; Pelland, N.; Mordy, C.W.; Cheng, W.; Kivva, K.; et al. Spring Phytoplankton Bloom Phenology during Recent Climate Warming on the Bering Sea Shelf. *Prog. Oceanogr.* **2024**, *220*, 103176. [CrossRef]
12. Racault, M.-F.; Le Quéré, C.; Buitenhuis, E.; Sathyendranath, S.; Platt, T. Phytoplankton Phenology in the Global Ocean. *Ecol. Indic.* **2012**, *14*, 152–163. [CrossRef]
13. Zhang, S.; Bai, Y.; He, X.; Jiang, Z.; Li, T.; Gong, F.; Yu, S.; Pan, D. Spatial and Temporal Variations in Sea Surface pCO2 and Air-Sea Flux of CO2 in the Bering Sea Revealed by Satellite-Based Data during 2003–2019. *Front. Mar. Sci.* **2023**, *10*, 1099916. [CrossRef]
14. Baker, M.R.; Kivva, K.K.; Pisareva, M.N.; Watson, J.T.; Selivanova, J. Shifts in the Physical Environment in the Pacific Arctic and Implications for Ecological Timing and Conditions. *Deep Sea Res. Part II Top. Stud. Oceanogr.* **2020**, *177*, 104802. [CrossRef]
15. Codispoti, L.A.; Kelly, V.; Thessen, A.; Matrai, P.; Suttles, S.; Hill, V.; Steele, M.; Light, B. Synthesis of Primary Production in the Arctic Ocean: III. Nitrate and Phosphate Based Estimates of Net Community Production. *Prog. Oceanogr.* **2013**, *110*, 126–150. [CrossRef]

16. Lomas, M.W.; Moran, S.B.; Casey, J.R.; Bell, D.W.; Tiahlo, M.; Whitefield, J.; Kelly, R.P.; Mathis, J.T.; Cokelet, E.D. Spatial and Seasonal Variability of Primary Production on the Eastern Bering Sea Shelf. *Deep. Sea Res. Part II Top. Stud. Oceanogr.* **2012**, *65–70*, 126–140. [CrossRef]
17. Lomas, M.W.; Eisner, L.B.; Gann, J.; Baer, S.E.; Mordy, C.W.; Stabeno, P.J. Time-Series of Direct Primary Production and Phytoplankton Biomass in the Southeastern Bering Sea: Responses to Cold and Warm Stanzas. *Mar. Ecol. Prog. Ser.* **2020**, *642*, 39–54. [CrossRef]
18. Rho, T.; Whitledge, T.E. Characteristics of Seasonal and Spatial Variations of Primary Production over the Southeastern Bering Sea Shelf. *Cont. Shelf Res.* **2007**, *27*, 2556–2569. [CrossRef]
19. Brown, Z.; van Dijken, G.; Arrigo, K. A Reassessment of Primary Production and Environmental Change in the Bering Sea. *J. Geophys. Res.* **2011**, *116*, C08014. [CrossRef]
20. Datsky, A.; Samoylenko, V.V. The Raw Materials of Water Biological Resources in the Russian Waters of the Bering Sea and Its Value. *Probl. Fish.* **2021**, *22*, 64–99. [CrossRef]
21. Overland, J.E.; Stabeno, P.J. Is the Climate of the Bering Sea Warming and Affecting the Ecosystem? *Eos Trans. Am. Geophys. Union.* **2004**, *85*, 309–312. [CrossRef]
22. Datsky, A.; Kulik, V.; Datskaya, S. The Dynamics of the Abundance of Commercial Fish in the Far Eastern Seas and Adjacent Areas of the Open Part of the Pacific Ocean and Factors Influencing It. *Tr. VNIRO* **2021**, *186*, 31–77. [CrossRef]
23. Dias, B.S.; McGowan, D.W.; Campbell, R.; Branch, T.A. Influence of Environmental and Population Factors on Prince William Sound Herring Spawning Phenology. *Mar. Ecol. Prog. Ser.* **2022**, *696*, 103–117. [CrossRef]
24. Ruggerone, G.T.; Nielsen, J.L. Evidence for Competitive Dominance of Pink Salmon (*Oncorhynchus gorbuscha*) over Other Salmonids in the North Pacific Ocean. *Rev. Fish. Biol. Fish.* **2004**, *14*, 371–390. [CrossRef]
25. Shevlyakov, E.A.; Dederer, N.A.; Ostrovsky, V.I.; Khen, G.V. Thermal Conditions in Marine Coastal Waters as a Favorable Factor for Formation of Extremely Strong Year Classes of Karaginsky Bay Pink Salmon. *Russ. J. Mar. Biol.* **2024**, *50*, 486–496. [CrossRef]
26. Baker, M.R.; Farley, E.V.; Danielson, S.L.; Mordy, C.; Stafford, K.M.; Dickson, D.M.S. Integrated Research in the Arctic—Ecosystem Linkages and Shifts in the Northern Bering Sea and Eastern and Western Chukchi Sea. *Deep Sea Res. Part II Top. Stud. Oceanogr.* **2023**, *208*, 105251. [CrossRef]
27. Frey, K.E.; Comiso, J.C.; Stock, L.V.; Young, L.N.C.; Cooper, L.W.; Grebmeier, J.M. A Comprehensive Satellite-Based Assessment across the Pacific Arctic Distributed Biological Observatory Shows Widespread Late-Season Sea Surface Warming and Sea Ice Declines with Significant Influences on Primary Productivity. *PLoS ONE* **2023**, *18*, e0287960. [CrossRef]
28. Emelin, P.O.; Maznikova, O.A.; Benzik, A.N.; Sheibak, A.Y.; Trofimova, A.O.; Orlov, A.M. Invader's Portrait: Biological Characteristics of Walleye Pollock *Gadus chalcogrammus* in the Western Chukchi Sea. *Deep Sea Res. Part II Top. Stud. Oceanogr.* **2022**, *206*, 105211. [CrossRef]
29. Stafford, K.; Farley, E.; Ferguson, M.; Kuletz, K.; Levine, R. Northward Range Expansion of Subarctic Upper Trophic Level Animals into the Pacific Arctic Region. *Oceanography* **2022**, *35*, 158–166. [CrossRef]
30. Axler, K.E.; Goldstein, E.D.; Nielsen, J.M.; Deary, A.L.; Duffy-Anderson, J.T. Shifts in the Composition and Distribution of Pacific Arctic Larval Fish Assemblages in Response to Rapid Ecosystem Change. *Glob. Change Biol.* **2023**, *29*, 4212–4233. [CrossRef]
31. Kivva, K.K.; Budyansky, M.V.; Uleysky, M.Y.u.; Prants, S.V. Analysis of the Spatiotemporal Variability of Pacific Water Propagation in the Sea of Okhotsk Based on the Lagrangian Approach. *Oceanology* **2024**, *64*, S48–S60. [CrossRef]
32. Langan, J.A.; Cunningham, C.J.; Watson, J.T.; McKinnell, S. Opening the Black Box: New Insights into the Role of Temperature in the Marine Distributions of Pacific Salmon. *Fish Fish.* **2024**, *25*, 551–568. [CrossRef]
33. Budyansky, M.V.; Kulik, V.V.; Kivva, K.K.; Uleysky, M.Y.u.; Prants, S.V. Lagrangian Analysis of Pacific Waters in the Sea of Okhotsk Based on Satellite Data in Application to the Walleye Pollock Fishery. *Izv. Atmos. Ocean. Phys.* **2022**, *58*, 1427–1437. [CrossRef]
34. Kivva, K.K.; Kubryakov, A.A. Seasonal and Interannual Variability of Chlorophyll-a Concentration in the Bering Sea Found from Satellite Data. *Izv. Atmos. Ocean. Phys.* **2021**, *57*, 1643–1657. [CrossRef]
35. Iida, T.; Saitoh, S.-I. Temporal and Spatial Variability of Chlorophyll Concentrations in the Bering Sea Using Empirical Orthogonal Function (EOF) Analysis of Remote Sensing Data. *Deep Sea Res. Part II Top. Stud. Oceanogr.* **2007**, *54*, 2657–2671. [CrossRef]
36. Waga, H.; Eicken, H.; Hirawake, T.; Fukamachi, Y. Variability in Spring Phytoplankton Blooms Associated with Ice Retreat Timing in the Pacific Arctic from 2003–2019. *PLoS ONE* **2021**, *16*, e0261418. [CrossRef]
37. Kivva, K.; Selivanova, J.; Pisareva, M.; Sumkina, A.A. Role of Physical Processes in Formation of Spring Phytoplankton Bloom in the Bering Sea. *Trudy VNIRO* **2020**, *181*, 206–222. [CrossRef]
38. Konik, M.; Angelica Peña, M.; Hirawake, T.; Hunt, B.P.V.; Suseelan Vishnu, P.; Eisner, L.B.; Bracher, A.; Xi, H.; Marchese, C.; Costa, M. Bioregionalization of the Subarctic Pacific Based on Phytoplankton Phenology and Composition. *Prog. Oceanogr.* **2024**, *228*, 103315. [CrossRef]
39. Chen, C.; Mao, Z.; Han, G.; Zhu, Q.; Gong, F.; Wang, T. Latitudinal and Interannual Variations of the Spring Phytoplankton Bloom Peak in the East Asian Marginal Seas. *Acta Oceanol. Sin.* **2016**, *35*, 81–88. [CrossRef]

40. Liu, Z.; Du, P.; Wang, Z.; Zhao, B.; Luo, W.; Yu, Z.; Yuan, L. Coastal Phytoplankton Blooms and Multivariate Analysis with Meteorological Factors and Climate Oscillation Signals in Western North Pacific. *Acta Oceanol. Sin.* **2024**, *43*, 85–101. [CrossRef]
41. Tskhay, Z.R.; Khen, G.V. Estimating the Total Concentration of Chlorophyll a in the Sea of Okhotsk Using Satellite Data. *Izv. Atmos. Ocean. Phys.* **2021**, *57*, 980–990. [CrossRef]
42. Zhao, H.; Matsuoka, A.; Manizza, M.; Winter, A. Recent Changes of Phytoplankton Bloom Phenology in the Northern High-Latitude Oceans (2003–2020). *J. Geophys. Res. Ocean.* **2022**, *127*, e2021JC018346. [CrossRef]
43. Naik, P.; D'Sa, E.J.; do Gomes, H.R.; Goés, J.I.; Mouw, C.B. Light Absorption Properties of Southeastern Bering Sea Waters: Analysis, Parameterization and Implications for Remote Sensing. *Remote Sens. Environ.* **2013**, *134*, 120–134. [CrossRef]
44. Salyuk, P.A.; Stepochkin, I.E.; Bukin, O.A.; Sokolova, E.B.; Mayor, A.Y.; Shambarova, J.V.; Gorbushkin, A.R. Determination of the Chlorophyll a Concentration by MODIS-Aqua and VIIRS Satellite Radiometers in Eastern Arctic and Bering Sea. *Izv. Atmos. Ocean. Phys.* **2016**, *52*, 988–998. [CrossRef]
45. Nicholson, S.-A.; Ryan-Keogh, T.J.; Thomalla, S.J.; Chang, N.; Smith, M.E. Satellite-Derived Global-Ocean Phytoplankton Phenology Indices. *Earth Syst. Sci. Data* **2025**, *17*, 1959–1975. [CrossRef]
46. Hunt, G.L., Jr.; Stabeno, P.; Walters, G.; Sinclair, E.; Brodeur, R.D.; Napp, J.M.; Bond, N.A. Climate Change and Control of the Southeastern Bering Sea Pelagic Ecosystem. *Deep Sea Res. Part II Top. Stud. Oceanogr.* **2002**, *49*, 5821–5853. [CrossRef]
47. Kahru, M.; Brotas, V.; Manzano-Sarabia, M.; Mitchell, B.G. Are Phytoplankton Blooms Occurring Earlier in the Arctic? *Glob. Change Biol.* **2011**, *17*, 1733–1739. [CrossRef]
48. Meier, W.; Fetterer, F.; Windnagel, A.; Stewart, J.S.; Stafford, T. *NOAA/NSIDC Climate Data Record of Passive Microwave Sea Ice Concentration*; (G02202, Version 5). [Data Set]; National Snow and Ice Data Center: Boulder, CO, USA, 2024. [CrossRef]
49. Thomalla, S.J.; Nicholson, S.-A.; Ryan-Keogh, T.J.; Smith, M.E. Widespread Changes in Southern Ocean Phytoplankton Blooms Linked to Climate Drivers. *Nat. Clim. Chang.* **2023**, *13*, 975–984. [CrossRef]
50. Kim, E.; Nam, S.-H.; Ahn, C.H.; Lee, S.; Koo, J.-W.; Hwang, T.-M. Comparison of Spatial Interpolation Methods for Distribution Map an Unmanned Surface Vehicle Data for Chlorophyll-a Monitoring in the Stream. *Environ. Technol. Innov.* **2022**, *28*, 102637. [CrossRef]
51. Lam, N.S.-N. Spatial Interpolation Methods: A Review. *Am. Cartogr.* **1983**, *10*, 129–150. [CrossRef]
52. Zhao, Z.; Xiao, R.; Guo, J.; Zhang, Y.; Zhang, S.; Lv, X.; Shi, H. Three-Dimensional Spatial Interpolation for Chlorophyll-a and Its Application in the Bohai Sea. *Sci. Rep.* **2023**, *13*, 7930. [CrossRef] [PubMed]
53. Alvera-Azcárate, A.; Barth, A.; Sirjacobs, D.; Lenartz, F.; Beckers, J.M. Data Interpolating Empirical Orthogonal Functions (DINEOF): A Tool for Geophysical Data Analyses. *Mediterr. Mar. Sci.* **2011**, *12*, 5–11. [CrossRef]
54. Beckers, J.M.; Rixen, M. EOF Calculations and Data Filling from Incomplete Oceanographic Datasets. *J. Atmos. Ocean. Technol.* **2003**, *20*, 1839–1856. [CrossRef]
55. Zhao, H.; Matsuoka, A.; Manizza, M.; Winter, A. DINEOF Interpolation of Global Ocean Color Data: Error Analysis and Masking. *J. Atmos. Ocean. Technol.* **2024**, *41*, 953–968. [CrossRef]
56. Ćatipović, L.; Matić, F.; Kalinić, H. Reconstruction Methods in Oceanographic Satellite Data Observation—A Survey. *J. Mar. Sci. Eng.* **2023**, *11*, 340. [CrossRef]
57. Taylor, M. Sinkr: Collection of Functions with Emphasis on Multivariate Data Analysis. 2025. Available online: https://github.com/marchtaylor/sinkr (accessed on 16 December 2025).
58. Banse, K.; English, D.C. Comparing Phytoplankton Seasonality in the Eastern and Western Subarctic Pacific and the Western Bering Sea. *Prog. Oceanogr.* **1999**, *43*, 235–288. [CrossRef]
59. Brody, S.R.; Lozier, M.S.; Dunne, J.P. A Comparison of Methods to Determine Phytoplankton Bloom Initiation. *J. Geophys. Res. Ocean.* **2013**, *118*, 2345–2357. [CrossRef]
60. Cole, H.; Henson, S.; Martin, A.; Yool, A. Mind the Gap: The Impact of Missing Data on the Calculation of Phytoplankton Phenology Metrics. *J. Geophys. Res. Ocean.* **2012**, *117*, C08030. [CrossRef]
61. Ferreira, A.; Mendes, C.R.B.; Costa, R.R.; Brotas, V.; Tavano, V.M.; Guerreiro, C.V.; Secchi, E.R.; Brito, A.C. Climate Change Is Associated with Higher Phytoplankton Biomass and Longer Blooms in the West Antarctic Peninsula. *Nat. Commun.* **2024**, *15*, 6536. [CrossRef]
62. Siegel, D.A.; Doney, S.C.; Yoder, J.A. The North Atlantic Spring Phytoplankton Bloom and Sverdrup's Critical Depth Hypothesis. *Science* **2002**, *296*, 730–733. [CrossRef]
63. R Core Team. *R: A Language and Environment for Statistical Computing, Version 4.5.2*; R Foundation for Statistical Computing: Vienna, Austria, 2024.
64. Pebesma, E.; Bivand, R. *Spatial Data Science: With Applications in R.*; Chapman and Hall/CRC: Boca Raton, FL, USA, 2023; ISBN 978-0-429-85944-1.
65. Wickham, H.; Averick, M.; Bryan, J.; Chang, W.; McGowan, L.; François, R.; Grolemund, G.; Hayes, A.; Henry, L.; Hester, J.; et al. Welcome to the Tidyverse. *J. Open Source Softw.* **2019**, *4*, 1686. [CrossRef]
66. Wickham, H.; François, R. *Dplyr: A Grammar of Data Manipulation*; R Foundation for Statistical Computing: Vienna, Austria, 2014.

67. Grolemund, G.; Wickham, H. Dates and Times Made Easy with Lubridate. *J. Stat. Softw.* **2011**, *40*, 1–25. [CrossRef]
68. Pebesma, E. Simple Features for R: Standardized Support for Spatial Vector Data. *R J.* **2018**, *10*, 439. [CrossRef]
69. Gräler, B.; Pebesma, E.; Heuvelink, G. Spatio-Temporal Interpolation Using Gstat. *R. J.* **2016**, *8*, 204. [CrossRef]
70. Wickham, H. *Ggplot2: Elegant Graphics for Data Analysis*, 2nd ed.; Use R! Springer: Cham, Switzerland, 2016; ISBN 978-3-319-24275-0.
71. Springer, A.M.; McROY, C.P.; Flint, M.V. The Bering Sea Green Belt: Shelf-Edge Processes and Ecosystem Production. *Fish. Oceanogr.* **1996**, *5*, 205–223. [CrossRef]
72. Ji, R.; Edwards, M.; Mackas, D.L.; Runge, J.A.; Thomas, A.C. Marine Plankton Phenology and Life History in a Changing Climate: Current Research and Future Directions. *J. Plankton Res.* **2010**, *32*, 1355–1368. [CrossRef]
73. Sambrotto, R.N.; Niebauer, H.J.; Goering, J.J.; Iverson, R.L. Relationships among Vertical Mixing, Nitrate Uptake, and Phytoplankton Growth during the Spring Bloom in the Southeast Bering Sea Middle Shelf. *Cont. Shelf Res.* **1986**, *5*, 161–198. [CrossRef]
74. Stabeno, P.J.; Bond, N.A.; Kachel, N.B.; Salo, S.A.; Schumacher, J.D. On the Temporal Variability of the Physical Environment over the South-eastern Bering Sea. *Fish. Oceanogr.* **2001**, *10*, 81–98. [CrossRef]
75. Nunes, G.S.; Ferreira, A.; Brito, A.C. Long-Term Satellite Data Reveals Complex Phytoplankton Dynamics in the Ross Sea, Antarctica. *Commun. Earth Env.* **2025**, *6*, 864. [CrossRef]
76. Sergeeva, V.M.; Stepanova, S.V.; Flint, M.V.; Sukhanova, I.N.; Fedorov, A.V.; Artemiev, V.A. Spatial and Seasonal Variability of Arctic Phytoplankton Communities in Conditions of Interaction with Atlantic Origin Waters in the St. Anna Trough (Kara Sea). *J. Mar. Syst.* **2025**, *249*, 104051. [CrossRef]
77. Basterretxea, G.; Font-Muñoz, J.S.; Hernández-Carrasco, I.; Sañudo-Wilhelmy, S.A. Global Variability of High-Nutrient Low-Chlorophyll Regions Using Neural Networks and Wavelet Coherence Analysis. *Ocean. Sci.* **2023**, *19*, 973–990. [CrossRef]
78. Kang, J.; Chen, X.; Zhang, M. The Distribution of Chlorophyll a and Its Influencing Factors in Different Regions of the Bering Sea. *Acta Oceanol. Sin.* **2014**, *33*, 112–119. [CrossRef]
79. Harrison, P.J.; Whitney, F.A.; Tsuda, A.; Saito, H.; Tadokoro, K. Nutrient and Plankton Dynamics in the NE and NW Gyres of the Subarctic Pacific Ocean. *J. Oceanogr.* **2004**, *60*, 93–117. [CrossRef]
80. Sasaoka, K.; Chiba, S.; Saino, T. Climatic Forcing and Phytoplankton Phenology over the Subarctic North Pacific from 1998 to 2006, as Observed from Ocean Color Data. *Geophys. Res. Lett.* **2011**, *38*, L15609. [CrossRef]
81. Konik, M.; Hunt, B.P.V.; Peña, M.A.; Hirawake, T.; Marchese, C.; Vishnu, P.S.; Bracher, A.; Xi, H.; Costa, M. Changes in Subarctic Pacific Phytoplankton Communities over the Last Two Decades. *Front. Mar. Sci.* **2025**, *12*, 1609094. [CrossRef]
82. Park, J.-W.; Kim, Y.; Kim, K.-W.; Fujiwara, A.; Waga, H.; Kang, J.J.; Lee, S.-H.; Yang, E.-J.; Hirawake, T. Contribution of Small Phytoplankton to Primary Production in the Northern Bering and Chukchi Seas. *Water* **2022**, *14*, 235. [CrossRef]
83. Kolomyts, E. Hierarchical System of Landscape-Geographial Spaces and Mechanisms of Its Formation. *Resour. Environ. Inf. Eng.* **2025**, *6*, 280–294. [CrossRef]
84. Jin, K.; Dong, C.; Liu, X.; Sun, Y.; Liu, J.; Lin, L. Phenological Characteristics of the Yellow Sea Spring Bloom: A Comparative Evaluation of Multiple Diagnostic Methods. *Remote Sens.* **2025**, *17*, 3106. [CrossRef]
85. Silva, E.; Counillon, F.; Brajard, J.; Korosov, A.; Pettersson, L.H.; Samuelsen, A.; Keenlyside, N. Twenty-One Years of Phytoplankton Bloom Phenology in the Barents, Norwegian, and North Seas. *Front. Mar. Sci.* **2021**, *8*, 746327. [CrossRef]
86. Liu, X.; Wang, M. Global Daily Gap-Free Ocean Color Products from Multi-Satellite Measurements. *Int. J. Appl. Earth Obs. Geoinf.* **2022**, *108*, 102714. [CrossRef]
87. Stock, A.; Subramaniam, A.; Van Dijken, G.L.; Wedding, L.M.; Arrigo, K.R.; Mills, M.M.; Cameron, M.A.; Micheli, F. Comparison of Cloud-Filling Algorithms for Marine Satellite Data. *Remote Sens.* **2020**, *12*, 3313. [CrossRef]
88. Suchy, K.D.; Le Baron, N.; Hilborn, A.; Perry, R.I.; Costa, M. Influence of Environmental Drivers on Spatio-Temporal Dynamics of Satellite-Derived Chlorophyll *a* in the Strait of Georgia. *Prog. Oceanogr.* **2019**, *176*, 102134. [CrossRef]
89. Zhou, G.; Liu, M.; Xu, L.; Li, L. A Gap-Filling Method for Satellite-Derived Chlorophyll-a Time Series Based on Neighborhood Spatiotemporal Information. *Int. J. Appl. Earth Obs. Geoinf.* **2024**, *128*, 103724. [CrossRef]
90. Fu, Y.; Zhu, Z.; Liu, L.; Zhan, W.; He, T.; Shen, H.; Zhao, J.; Liu, Y.; Zhang, H.; Liu, Z.; et al. Remote Sensing Time Series Analysis: A Review of Data and Applications. *J. Remote Sens.* **2024**, *4*, 0285. [CrossRef]
91. Corredor-Acosta, A.; Morales, C.E.; Hormazabal, S.; Andrade, I.; Correa-Ramirez, M.A. Phytoplankton Phenology in the Coastal Upwelling Region off Central-Southern Chile (35°S–38°S): Time-space Variability, Coupling to Environmental Factors, and Sources of Uncertainty in the Estimates. *J. Geophys. Res. Ocean.* **2015**, *120*, 813–831. [CrossRef]
92. Henson, S.A.; Cole, H.S.; Hopkins, J.; Martin, A.P.; Yool, A. Detection of Climate Change-driven Trends in Phytoplankton Phenology. *Glob. Change Biol.* **2018**, *24*, 101–111. [CrossRef]
93. Biliani, I.; Skamnia, E.; Economou, P.; Zacharias, I. A Novel Methodology to Correct Chlorophyll-a Concentrations from Satellite Data and Assess Credible Phenological Patterns. *Remote Sens.* **2025**, *17*, 1156. [CrossRef]

94. Malysheva, A.S.; Lobanova, P.V. Interannual Variability of Marine Phytoplankton Spring Bloom Phenology in the North European Basin. *Oceanology* **2024**, *64*, S107–S117. [CrossRef]
95. Platt, T.; White, G.N.; Zhai, L.; Sathyendranath, S.; Roy, S. The Phenology of Phytoplankton Blooms: Ecosystem Indicators from Remote Sensing. *Ecol. Model.* **2009**, *220*, 3057–3069. [CrossRef]
96. Vikebø, F.B.; Strand, K.O.; Sundby, S. Wind Intensity Is Key to Phytoplankton Spring Bloom Under Climate Change. *Front. Mar. Sci.* **2019**, *6*, 444060. [CrossRef]
97. Ueyama, R.; Monger, B.C. Wind-Induced Modulation of Seasonal Phytoplankton Blooms in the North Atlantic Derived from Satellite Observations. *Limnol. Oceanogr.* **2005**, *50*, 1820–1829. [CrossRef]

Disclaimer/Publisher's Note: The statements, opinions and data contained in all publications are solely those of the individual author(s) and contributor(s) and not of MDPI and/or the editor(s). MDPI and/or the editor(s) disclaim responsibility for any injury to people or property resulting from any ideas, methods, instructions or products referred to in the content.